Received: 3 July 2023 | Revised: 1 September 2023 | Accepted: 22 September 2023

IET Control Theory & Applications

DOI: 10.1049/cth2.12565

The Institution of Engineering and Technology WILEY

ORIGINAL RESEARCH

Nonlinear impedance matching control for a submerged wave energy converter

Alejandro Gonzalez-Esculpi[1] | **Cristina Verde**[1] | **Paul Maya-Ortiz**[2]

[1]Instituto de Ingeniería, Universidad Nacional Autónoma de México, Mexico City, Mexico

[2]Facultad de Ingeniería, Universidad Nacional Autónoma de México, Mexico City, Mexico

Correspondence
Alejandro Gonzalez-Esculpi, Instituto de Ingeniería, Universidad Nacional Autónoma de México, Av. Universidad 3004, Coyoacán, Mexico City 04510, Mexico.
Email: alejandro96z@gmail.com

Funding information
Universidad Nacional Autónoma de México: Programa de Apoyo a Proyectos de Investigación e Innovación Tecnológica 415 (PAPIIT-UNAM), Grant/Award Numbers: IT100122, B221581; Consejo Nacional de Ciencia y Tecnología (CONACyT), Grant/Award Number: CVU 925686

Abstract

The impedance matching control, also known as approximate complex conjugate control (ACC), is one of the main strategies for improving the capture of energy by point absorber wave energy converters. Such a strategy shapes the mechanical impedance related to the floater dynamics via the control law. Since the traditional ACC is given by a linear control law, this work proposes a generalization denoted as nonlinear complex conjugate control (NCC) that considers the presence of nonlinear viscous damping in addition to the usual linear damping and stiffness. The energy maximization conditions for the proposed NCC are derived in the frequency domain through the describing function method. These conditions show that the ACC is a special case of the NCC when the total damping on the floater is approximated as a linear function of its velocity. From numerical simulations of a point absorber wave energy converters with nonlinear damping, which is based on the Archimedes wave swing prototype, it is shown that the NCC provides greater energy conversion than the ACC, as well as a robust performance in the presence of variations of the damping coefficient and the excitation force peak frequency.

1 | INTRODUCTION

Control systems play a key role in maximizing the efficiency of wave energy converters (WECs), as can be seen in several alternatives for this objective proposed and studied since 1976 [1]. For WECs based on floaters of negligible dimensions with respect to the wavelength of the sea wave, which are classified as point absorbers (PA-WECs), a fundamental contribution for maximizing the converted energy is given by the phase and amplitude conditions established by Falnes [2]. By considering a floater with linear dynamics with vertical motion caused by the sea waves, the phase condition is fulfilled if the velocity of the floater is in phase with the respective excitation force, while the amplitude condition indicates the total damping required for the floater motion.

Since most of the control schemes for PA-WECs are based on the phase and amplitude conditions mentioned above, Hals et al. [3] established two main approaches: approximate velocity tracking (AVT) and approximate complex conjugate control (ACC). AVT-based schemes aim to track a reference velocity for the floater proportional to the excitation force. These schemes have been considered with strategies such as internal model control using neural networks [4], adaptive control [5], and model predictive control (MPC) [6]. On the other hand, ACC-based schemes seek to adjust the mechanical impedance related to the floater motion as follows: (i) the phase condition is fulfilled by matching the resonance frequency with that of the waves. Furthermore, (ii) the amplitude condition is achieved by shaping the mechanical damping. Some applications of this approach can be seen in Wu et al. [7] for a fully submerged WEC and Hansen [8] for a WEC composed of multiple absorbers. In addition, Song et al. [9] showed another application of ACC by proposing a scheme that provides resonance at multiple frequencies.

Even though the AVT-based schemes may perform better in the presence of panchromatic sea waves, the construction of the reference velocity requires a real-time estimate of the excitation force. This can be a difficult task that involves predicting the behavior of the sea wave [10, 11]. Conversely, ACC-based schemes generally depend more on the frequency of the incident sea wave but without requiring estimates of the excitation

Abbreviations: ACC, approximate complex conjugate control; DFM, describing function method; NCC, nonlinear complex conjugate control; WEC, wave energy converter.

force. These facts justify that ACC-based schemes might be adequate for practical applications when a simple design is desired under the assumption of sea waves with a quasi-stationary dominant frequency.

The conditions for maximizing the capture of energy by the WEC established by Falnes [2] suppose unconstrained motion of the floater described by linear dynamics excited by monochromatic sea waves. The actual dynamics of the floater excited by sea waves, however, involve nonlinear components that cause the phenomena below.

- Physical boundaries on the floater motion and the actuator. The causes are associated with the constraints on the motion of the floater as well as the mechanical and electrical signals in the generator. These conditions have been addressed by model predictive control schemes [12, 13].
- Variations on the wet surface of the floater. The situation produced by variations on the submerged surface of the floater is represented in the model as a nonlinear stiffness force governed by the floater position. Nielsen et al. [14] tackled this issue by proposing an ACC-based scheme.
- Viscous damping. This situation is usually modeled by a quadratic function of the floater velocity [15, 16], and the drag force caused by the flow of water is indicated as the main cause. The importance of considering the nonlinear force caused by viscous damping for maximizing the energy conversion, even in the absence of motion limitations, has been demonstrated by Mérigaud and Ringwood [17]. A special case can be found in the 2004 Archimedes wave swing (AWS) prototype, where the nonlinear damping is mainly caused by a set of brakes included for protecting the structure from extreme forces on the sea bottom [18].

Since most of the ACC-based strategies for WECs reported in the literature do not address the nonlinear phenomena indicated above, the main contribution presented here is a generalization of the ACC that takes into account the nonlinear damping effect in a submerged PA-WEC. The proposed scheme, denoted here as nonlinear complex conjugate control (NCC), incorporates a nonlinear damping term in addition to the typical adjustment of linear stiffness and linear damping used for the ACC. A procedure for adjusting the gains of the proposed controller is developed by applying the describing function method (DFM) [19, 20], which approximates the nonlinear functions as linear ones that depend on the frequency.

It is worth noting that the DFM allows using diverse common techniques for the analysis and design of closed-loop systems. The applicability of the DFM depends on the fulfillment of low-pass filtering conditions of the system so that a unique dominant frequency governs its sinusoidal steady-state response [19, 20]. Thus, the suitability of the DFM for the energy maximization objective comes from the usual characterization of irregular sea waves, which according to Faltinsen [21] is given by random signals with a narrow band quasi-stationary power spectrum around a peak frequency.

To develop and analyze the proposed control law, a PA-WEC based on the model of the AWS experimentally verified in [18] is considered as the case study. Two reasons motivated the selection of this particular WEC device: (i) the important effects on the braking subsystem that generate nonlinear damping forces in the floater, and (ii) the availability of the detailed model with parameter values. In addition, this WEC allows implementing the desired impedance matching by performing a mechanical adjustment of the resonance frequency of the floater motion and by shaping the damping through the generator.

By considering the approximate frequency response of the closed-loop system, one derives the conditions of the NCC gains for maximizing the average converted power. Two conditions are obtained: one for the stiffness coefficient and another that establishes a relation between the linear and nonlinear damping gains. By analyzing the results with the proposed control, one can observe that in the absence of viscous damping on the floater the adjustment of the NCC gains is similar to the one corresponding to the ACC. These facts allow one to strongly consider the NCC as a generalization of the ACC. In addition, the extreme case in which the external damping on the floater is mostly nonlinear is also analyzed.

The proposed control strategy and the adjustment procedure were validated here with numerical simulations that contemplate regular (monochromatic) and irregular (panchromatic) sea waves. Two synthetic experiments were performed. First, the proposed NCC was compared with the traditional ACC by analyzing the transient evolution of the floater velocity and the instantaneous converted power. The results showed that the system with NCC provides a greater average converted power than the one with ACC. Second, the sinusoidal steady-state regime of the system with NCC was analyzed given the nominal tuning of the control in the presence of deviations of the values of the damping coefficient of the brakes as well as the peak frequency of the incident sea waves. The results showed that for variations up to 25% of the peak frequency the variation of the average converted power is below 5% of its value in nominal condition.

The paper is structured as follows. Section 2 presents a description of the WEC and the floater dynamics. Section 3 presents the NCC control law, as well as the derivation of the conditions for maximizing the converted energy from the approximate frequency response obtained from the describing function method. Finally, the validation of the proposal from numerical simulations and the conclusions of the work are presented in Sections 4 and 5, respectively.

2 | WEC DESCRIPTION

A WEC based on the 2004 Archimedes wave swing (AWS) prototype [18] is considered here, which can be classified as a fully submerged device [22]. It operates on the sea bottom, with a floater that covers an air-filled central tank. The floater moves vertically according to the forces produced by the enclosed air and the excitation force $F_w(t)$ produced by the sea waves.

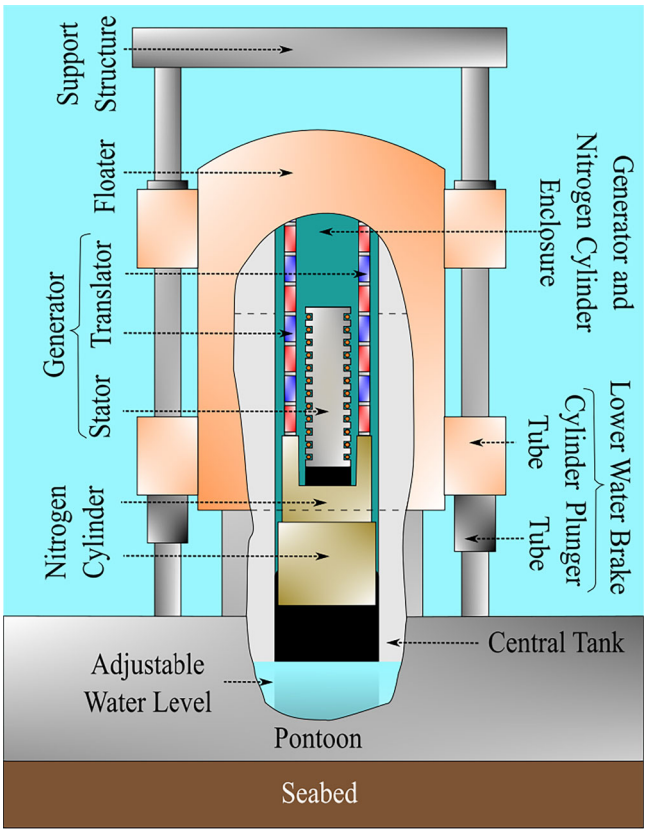

FIGURE 1 Main components of the structure of the WEC (not to scale).

In the full-scale prototype of the WEC tested in 2004, the floater is surrounded by a structure that restricts its motion within a range of 9 m. The main elements of the device are shown in Figure 1. The central tank filled with air and water acts as an air spring, and the nitrogen cylinder acts as a secondary spring. Furthermore, the upper and lower braking subsystems provide the required damping, and the linear generator produces the electrical energy from the floater motion. In addition, the pontoon contains water pumps and a subsystem of air and water pipes with secondary tanks for adjusting the middle position of the floater z_0 and its resonance frequency ω_r.

The linear permanent magnet generator (LPMG) is composed of a permanent magnet translator attached to the floater and a stator fixed inside the central tank. Thus, the three-phase stator can be connected to the generator side of a back-to-back converter [7] to fulfill the requirements of the electric grid.

2.1 | Floater dynamics

From [2], the dynamics of the floater restricted to vertical motion are described by

$$m_f \dot{v}(t) = F_k(z(t)) + F_b(v(t)) + F_r(v(t), \dot{v}(t)) + F_{gen}(t) + F_w(t), \quad (1)$$

where $z(t)$, $v(t)$, and $\dot{v}(t)$ represent the position, velocity, and acceleration of the floater with mass m_f. The remaining terms represent the forces that act on the floater, which are described below for the WEC under study.

- The excitation force $F_w(t)$ is caused by the sea waves and is directly related to the amount of converted energy. The relation between the wave elevation at the location of the floater $\eta_w(t)$ and $F_w(t)$ is modelled through [10, 11]:

$$F_w(t) = \int_{-\infty}^{\infty} h_w(t-\tau)\eta_w(\tau)\, d\tau, \quad (2)$$

where $h_w(t)$ denotes the excitation force impulse response function. Consider the assumptions below.
A1: The floater is a truncated cylinder with vertical axis.
A2: The water depth is infinite.
Under both assumptions, the frequency response related to $h_w(t)$ is given by [2]:

$$H_w(\omega) = \mathcal{F}\{h_w(t)\} = -S_f \rho g \exp\left(-\frac{\omega^2}{g} d_f\right), \quad (3)$$

where d_f is the depth of the floater with respect to the water level, ρ is the seawater density, g is the gravitational acceleration, S_f the area of the floater's top, ω the angular frequency variable, and $\mathcal{F}\{\cdot\}$ the Fourier transform operator.

For irregular sea waves, $\eta_w(t)$ is characterized by a power spectrum $S(\omega)$ related to a quasi-stationary sea state [21]. Given a frequency interval $[\omega_{min}, \omega_{max}]$ where $S(\omega)$ is assumed to be sufficiently significant, the excitation force can be described through

$$F_w(t) = \sum_{i=1}^{N} |H_w(\omega_i)| \eta_i \sin(\omega_i t + \varphi_i + \angle H(\omega_i)), \quad (4)$$

where the values of $\omega_i \in [\omega_{min}, \omega_{max}]$ represent N successive frequencies separated by $\delta\omega = (\omega_{max} - \omega_{min})/(N-1)$. In addition, $\eta_i = \sqrt{2\, S(\omega_i)\delta\omega}$ and φ_i are the amplitude and the phase shift, respectively, of the ith harmonic of $\eta_w(t)$. The random nature of the irregular sea wave is represented by the phase shifts φ_i, as each of them is a random variable characterized by a uniform distribution in $[-\pi, \pi)$ given a sea state defined by the parameters of $S(\omega)$. According to [11, 23], the power spectrum $S(\omega)$ is considered quasi-stationary since the variations of the sea state last between 30 min and 3 h, while the typical periods of the sea waves possess values between 5 and 15 s.

In this work, the JONSWAP power spectrum [21] is considered, which is given by

$$S(\omega) = 320.38 \frac{H_1^2}{T_w^4 \omega^5} \exp\left(-\frac{1951.23}{T_w^4 \omega^4}\right) 3.3^{Y(T_w,\omega)}, \quad (5)$$

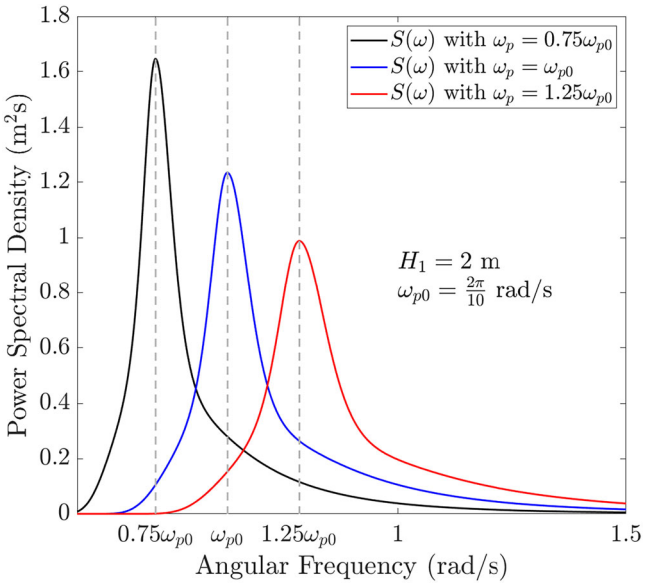

FIGURE 2 JONSWAP power spectrum with $H_1 = 2$ m and ±25% deviations of the peak frequency ω_p with respect to $\omega_{p0} = 2\pi/10$.

where

$$T_w = \frac{2\pi}{\omega_p},$$

$$Y(T_w, \omega) = \exp\left\{-\left(\frac{0.159\omega T_w - 1}{\sqrt{2}\sigma}\right)^2\right\},$$

$$\sigma = \begin{cases} 0.07 & \text{for} \quad \omega \le 6.28/T_w, \\ 0.09 & \text{for} \quad \omega > 6.28/T_w. \end{cases}$$

The peak frequency ω_p (i.e. the value of ω that maximizes $S(\omega)$) and the significant wave height H_1 are parameters related to the quasi-stationary sea state. One can note in (5) that the value of H_1 affects $S(\omega)$ uniformly at all the frequencies. On the other hand, the value of ω_p affects the bandwidth and the maximum value of $S(\omega)$. This can be seen in Figure 2, which shows $S(\omega)$ for $H_1 = 2$ m and different values of ω_p around $\omega_{p0} = 2\pi/10$ rad/s.

- The radiation force $F_r(v(t), \dot{v}(t))$ is produced by the oscillation of the floater in the absence of an incident wave. It depends on the geometry of the floater, and, for complex geometries, it is computed from experiments or computational flow dynamics software (e.g. WAMIT [24], NEMOH [25]). According to Falnes [2], this force is related to the floater velocity and acceleration through

$$F_r(v(t), \dot{v}(t)) = -\int_0^\infty h_r(t-\tau)v(\tau)d\tau - m_\infty \dot{v}(t), \quad (6)$$

where $h_r(t)$ denotes the radiation force impulse response function and m_∞ denotes the added mass at infinite frequency, which are given by

$$h_r(t) = \begin{cases} 0 & \text{for} \quad t < 0, \\ \mathcal{F}^{-1}\{2b_r(\omega)\} & \text{for} \quad t \ge 0, \end{cases} \quad (7)$$

$$m_\infty = \lim_{\omega\to\infty} m_r(\omega). \quad (8)$$

The variables $m_r(\omega)$ and $b_r(\omega)$ represent the added mass and the radiation resistance, respectively, caused by harmonic oscillations of the floater at an angular frequency ω in the absence of an incident sea wave. Under the assumptions 2.1 and 2.1, Falnes [2] describes the frequency response related to $h_r(t)$ through

$$H_r(\omega) = \mathcal{F}\{h_r(t)\} = b_r(\omega) + j\omega[m_r(\omega) - m_\infty], \quad (9)$$

where j denotes the imaginary unit. Falnes [2] also relates $b_r(\omega)$ with $H_w(\omega)$ through

$$b_r(\omega) = \frac{\omega^3 |H_w(\omega)|^2}{2\rho g^3}. \quad (10)$$

- The damping force $F_b(v(t))$ is produced by the braking subsystems that help to avoid a large stroke of the floater, the action of the bearing plates in the structure, and the drag effect produced by the water surrounding the floater. By only considering the effect of the brakes and neglecting the others, this force is represented by

$$F_b(v(t)) = -\beta v(t)|v(t)|, \quad (11)$$

where β represents the damping coefficient and $|\cdot|$ is the absolute value operator. It may be noted that for other WECs, as can be seen in [16], the characterization of viscous drag is similar to (11).

- The stiffness force $F_k(z(t))$ summarizes the effects of the weight of the floater $-m_f g$, the force related to the hydrostatic pressure $F_{hs}(z(t))$, the force produced by the air inside the central tank $F_{air}(z(t))$, and the force caused by the nitrogen cylinder $F_{nitro}(z(t))$. Thus,

$$F_k(z(t)) = -m_f g + F_{hs}(z(t)) + F_{air}(z(t)) + F_{nitro}(z(t)). \quad (12)$$

From experimental results, Prado et al. [18] approximated the total effect of this force as

$$F_k(z(t)) \approx -k_s z(t), \quad (13)$$

where k_s denotes the mechanical stiffness coefficient, which depends on the adjustable water level inside the central tank h_{ct} as well as the pressure caused by the air and water column on the top of the floater. Thus, its value is given by

$$k_s = -\rho g S_f + \gamma S_f^2 \frac{p_a^0}{V_{a0} - S_f h_{ct}} + \gamma S_n^2 \frac{p_n^0}{V_n^0}, \quad (14)$$

where $\gamma = 1.4$ is the heat capacity ratio, p_a^0 is the average air pressure inside the central tank, V_{a0} is the total volume of the central tank for the floater in the middle position $z = 0$,

S_n is the base area of the nitrogen cylinder, and p_n^0 as well as V_n^0 are the nitrogen pressure and volume at $z = 0$. It is worth noting that the mechanical adjustment of k_s involves pumping mechanisms.

- The generator force $F_{gen}(t)$ is related to the three-phase currents of the generator stator and the flux linkage of the permanent magnet in the translator [7]. These currents can be shaped through a field-oriented control scheme applied through the stator voltages on the generator side of an active load. Therefore, the generator force can be manipulated in order to track a reference $u(t)$. Since the generator dynamics are considerably faster than those of the floater, in this work one considers

$$F_{gen}(t) \approx u(t), \tag{15}$$

where $u(t)$ is shaped in order to affect the motion of the floater. As can be seen in [23], this approximation is frequently used in the study of control systems for WECs.

By considering Equations (6), (11), (13), and (15) and by defining $m = m_f + m_\infty$ as the total mass of the floater, the dynamics of the system (1) can be represented through

$$\begin{aligned} \dot{z}(t) &= v(t), \\ \dot{v}(t) &= \frac{1}{m}\left\{ -k_s z(t) - \beta v(t)|v(t)| - \mu_r(t) + u(t) + F_w(t) \right\}, \end{aligned} \tag{16}$$

where

$$\mu_r(t) = \int_0^\infty h_r(t-\tau)v(\tau)\,d\tau.$$

3 | MAXIMIZATION OF THE CONVERTED ENERGY

3.1 | Problem formulation

According to Ringwood et al. [23], the approximate complex conjugate control (ACC) strategy consists of maximizing the average power

$$P = -\frac{1}{T}\int_T u(t)v(t)\,dt \tag{17}$$

in sinusoidal steady state during a sufficiently long time period T by adjusting the mechanical impedance of the WEC. This can be achieved by shaping the generator force as depicted in Figure 3.

Ringwood et al. [23] indicated that the control law for ACC can be given by a linear function of the position and the velocity of the floater. Such a solution allows one to maximize the energy converted by WECs with linear dynamics. The proposed control law presented here, however, aims to tackle the nonlinear damping produced by the brakes by including a

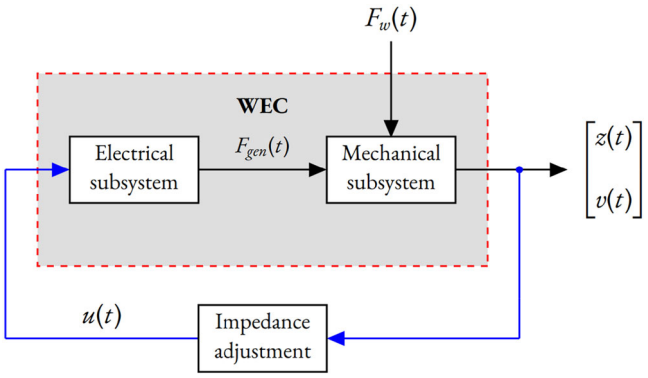

FIGURE 3 Scheme for approximate complex conjugate control of the WEC.

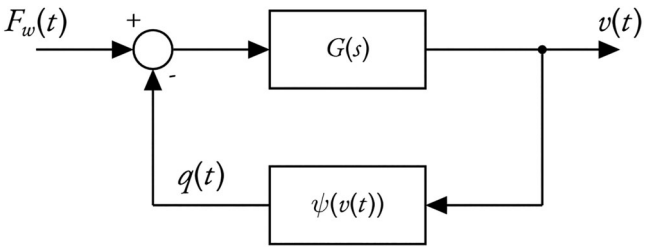

FIGURE 4 Interconnection of linear and nonlinear dynamics of the floater motion.

nonlinear function of the floater velocity. Hence, the proposed control law is parameterized as

$$u(t) = -k_g z(t) - b_g v(t) - \beta_g v(t)|v(t)|, \tag{18}$$

where the gains b_g and β_g shape the damping of the floater and can be assigned through different criteria, while k_g allows complementing the total stiffness force $F_k(z(t))$.

By considering the model (16) and the control law (18), the feedback system can be represented with the block diagram shown in Figure 4, where the system is approximated by a linear subsystem given by the transfer function

$$G(s) = \frac{s}{ms^2 + [H_r(s) + b_g]s + k}, \tag{19}$$

where $k = k_s + k_g$ and $H_r(s) = \mathcal{L}\{h_r(t)\}$, and, by the nonlinear terms grouped in the function

$$\psi(v(t)) = (\beta + \beta_g)v(t)|v(t)|. \tag{20}$$

Thus, the proposed design procedure for the ACC scheme consists of designing k, b_g, and β_g such that P is maximized given an approximate frequency response of the closed-loop system shown in Figure 4. To this end, one considers the describing function method (DFM) [19, 20], which approximates the behaviour of $\psi(v(t))$ in sinusoidal steady state under the assumption of a monochromatic excitation force given by

$$F_w(t) = F\sin(\omega_p t) \tag{21}$$

with a constant amplitude F. In the presence of irregular sea waves, the main condition for the validity of (21) is a narrow bandwidth around a unique frequency ω_p of the respective power spectrum $S(\omega)$. In the case of the JONSWAP power spectrum with a peak frequency $\omega_{p0} = 2\pi/10$ rad/s depicted in Figure 2, this work considers that the bandwidth is narrow enough. Therefore, the monochromatic sea wave assumption is used for determining an approximate frequency response related to the floater dynamics.

The specific describing function of $\psi(v(t))$ is developed in the following subsection in order to obtain an approximate frequency response of the WEC.

3.2 | Approximate frequency response of the WEC

The main supposition for obtaining an approximation of the function $\psi(v(t))$ is that the filtering properties of $G(s)$ impose a unique dominant frequency in the loop by attenuating the harmonics caused by the nonlinear term. Thus, for ω around the resonance frequency ω_r of $G(s)$, the floater velocity in sinusoidal steady state can be written as

$$v(t) \approx V \sin(\omega t + \varphi), \tag{22}$$

where $V > 0$ represents the amplitude of the floater velocity and φ its phase shift with respect to $F_w(t)$. In this condition, the signal at the output of the nonlinear block results in

$$q(t) = \sum_{i=0}^{\infty} Q_i \sin(i\omega t + \vartheta_i), \tag{23}$$

where $Q_i \geq 0$ and ϑ_i are the amplitude and the phase shift of the ith harmonic of the Fourier series representation of q. The approximation (22) is justified since $G(s)$ is a band-pass filter centered at ω_r, and only the first harmonic dominates in the system output. Thus, the nonlinear term can be approximated as

$$\psi(v(t)) \approx \Psi(V) v(t), \tag{24}$$

where $\Psi(V)$ represents the describing function of $\psi(v(t))$, which is taken from [20]:

$$\begin{aligned}\Psi(V) &= \frac{2\omega}{\pi V}\int_0^{\frac{\pi}{\omega}} (\beta + \beta_g) V^2 \sin(\omega t - \varphi)|\sin(\omega t - \varphi)|\sin(\omega t)\, dt \\ &= \frac{8}{3\pi}(\beta + \beta_g) V.\end{aligned} \tag{25}$$

Hence, from the interconnection of $G(s)$ and $\Psi(V)$, the amplitudes V and F are related in sinusoidal steady state through

$$\frac{V}{F} = \frac{\omega}{\sqrt{[k - m_T(\omega)\omega^2]^2 + \omega^2[b_T(\omega) + \frac{8}{3\pi}\beta_T V]^2}}, \tag{26}$$

where

$$\begin{aligned} m_T(\omega) &= m_f + m_r(\omega), \\ b_T(\omega) &= b_r(\omega) + b_g, \\ \beta_T &= \beta + \beta_g, \end{aligned} \tag{27}$$

and the phase shift is given by

$$\varphi = \frac{\pi}{2} - \angle\left\{k - m_T(\omega)\omega^2 + j\omega\left[b_T(\omega) + \frac{8}{3\pi}\beta_T V\right]\right\}, \tag{28}$$

where $\angle\phi$ is the phase angle of the complex number ϕ.

By accommodating the terms of (26), one obtains

$$f(V) - F\omega = 0, \tag{29}$$

where

$$f(V) = V\sqrt{\left[k - m_T(\omega)\omega^2\right]^2 + \omega^2\left[b_T(\omega) + \frac{8}{3\pi}\beta_T V\right]^2}. \tag{30}$$

Since $\partial f(V)/\partial V > 0$ for all $V > 0$ for any set of parameters of the system, $f(V)$ is a monotonically increasing function of V and also satisfies $f(0) = 0$ as well as $f(V) \to \infty$ for $V \to \infty$. These facts allow establishing that (29) has a unique positive solution of V, which together with φ defines the approximate frequency response of the WEC.

The unique positive real value of V can be computed from (29) through numerical methods for nonlinear equations. As an alternative for obtaining V, one can solve the following polynomial equation derived from (26):

$$a_4 V^4 + a_3 V^3 + a_2 V^2 + a_1 V + a_0 = 0, \tag{31}$$

with

$$\begin{aligned} a_0 &= -\frac{9\pi^2}{64}F^2, \\ a_1 &= 0, \\ a_2 &= \left(\frac{9\pi^2}{64}\right)\frac{b_T^2(\omega)\omega^2 + [k - m_T(\omega)\omega^2]^2}{\omega^2}, \\ a_3 &= \frac{3\pi}{4}b_T(\omega)(\beta + \beta_g), \\ a_4 &= (\beta + \beta_g)^2. \end{aligned} \tag{32}$$

Equation (31) is satisfied by four values of V that depend on the parameters of the system and the excitation force, but only the real positive value that also satisfies (29) has a physical meaning. The coefficients in (32) are useful for determining the conditions for the maximization of P, as shown in the following subsection.

3.3 | Conditions for maximizing the average converted power

The starting point for maximizing the converted energy consists of determining the average converted power P in terms of the parameters to be optimized. Hence, by considering the approximate velocity (22) and the control law (18), for $T = 2\pi/\omega$, P is reduced to

$$P \approx \frac{1}{2} b_g V^2 + \frac{4}{3\pi} \beta_g V^3. \tag{33}$$

According to the ACC strategy, as mentioned above, the maximization of P is performed by adjusting the stiffness and the damping on the floater. This means the condition

$$\frac{\partial P}{\partial k} = 0, \ \frac{\partial P}{\partial b_g} = 0, \ \frac{\partial P}{\partial \beta_g} = 0 \tag{34}$$

must be satisfied.

For the stiffness coefficient k, by the chain rule,

$$\frac{\partial P}{\partial k} = \frac{\partial P}{\partial V} \frac{\partial V}{\partial k} = 0. \tag{35}$$

Thus, the value set of k is obtained from the condition

$$\frac{\partial V}{\partial k} = 0. \tag{36}$$

To obtain the value set of k that satisfies (36) without determining $V > 0$, one uses the following fact.

Fact 1 [26]. *Consider the nth order polynomial equation*

$$\sum_{i=0}^{n} a_i(\theta) V^i = 0, \tag{37}$$

where each coefficient $a_i(\theta)$ is a differentiable function of the set of parameters

$$\theta = [\theta_1 \ \cdots \ \theta_m]^\top. \tag{38}$$

Thus, the partial derivative of the lth root of (37) with respect to the qth parameter θ_q is given by

$$\frac{\partial V_l}{\partial \theta_q} = -\frac{\sum_{i=0}^{n} \left(\frac{\partial a_i}{\partial \theta_q} \right) V_l^i}{\sum_{i=0}^{n} i a_i V_l^{i-1}}. \quad \blacksquare \tag{39}$$

Therefore, from the set of coefficients (32), one obtains

$$\frac{\partial a_2}{\partial k} = \left(\frac{9\pi^2}{32} \right) \frac{k - m_T(\omega)\omega^2}{\omega^2}, \qquad \frac{\partial a_i}{\partial k} = 0 \quad \text{for } i \neq 2, \tag{40}$$

and P is maximized if

$$k = k_0 = m_T(\omega_p)\, \omega_p^2, \tag{41}$$

where ω_p is the assumed frequency of the incident sea wave. The condition (41) means that ω_r should be synchronized with ω_p, which corresponds to the phase condition for maximum power absorption by a floater with linear dynamics given in [2]. This condition also coincides with the suggestion reported in [7, 18] for the WEC under study; neither cited work used the DFM for such an adjustment. Therefore, the resulting value of V is

$$V|_{k=k_0} = \frac{-3\pi b_T(\omega_p) + \sqrt{9\pi^2 b_T^2(\omega_p) + 96\pi\beta_T F}}{16\beta_T}. \tag{42}$$

Thus, the condition for maximizing P with respect to b_g and β_g obtained from (42) and (33) is given by

$$b_g = \frac{(2\beta - \beta_g)\sqrt{\pi b_r^2(\omega_p) + 8F\beta} + \sqrt{\pi} b_r(\omega_p)(\beta + \beta_g)}{3\beta\sqrt{\pi}}. \tag{43}$$

It is worth noting that the adjustment of k and b_g given by the conditions (41) and (43) should be updated if ω_p varies. In the presence of irregular sea waves ω_p might represent the peak frequency of the power spectrum related to the quasi-stationary sea state.

The derived conditions for maximizing the converted energy are the basis for shaping the mechanical impedance of the floater described in the following subsection.

3.4 | Mechanical impedance matching

To maximize the converted energy, the first step is to assign the value of $k = k_s + k_g$ such that the stiffness condition (41) is satisfied. One must then assign the values of β_g and b_g to satisfy the damping condition (43). Thus, one may consider the following alternatives for adjusting the parameters of the control law (18).

- A first option is given by the traditional approximate complex conjugate control (ACC) [23] that only considers a linear function of the position and the velocity of the floater (i.e. $\beta_g^{ACC} = 0$). Thus, one obtains

$$b_g^{ACC} = \frac{2\sqrt{\pi b_r^2(\omega_p) + 8F\beta} + \sqrt{\pi} b_r(\omega_p)}{3\sqrt{\pi}}. \tag{44}$$

  Clearly, a disadvantage of this adjustment of the linear gain is that it requires an estimate of F. It is worth noting that this tuning of the damping injected into the floater dynamics represents an alternative to the one proposed by Wu et al. [7] for an AWS-based WEC.
- A second option is given by assigning $\beta_g = -\beta$ to impose linear damping on the floater dynamics. This is considered as

an inconvenient solution because of the following: (i) from (33) the average converted power is a positive monotonically increasing function of the floater velocity if and only if the values of b_g and β_g are positive. Furthermore, (ii) a negative value of β_g can make the system unstable if the value of β is not properly estimated, as the total nonlinear damping may become negative.

- A third option is given by choosing β_g such that b_g becomes independent of the value of F. Thus, the obtained adjustment of the gains is given by

$$\beta_g^{NCC} = 2\beta \quad \text{and} \quad b_g^{NCC} = b_r(\omega_p), \tag{45}$$

where the superscript NCC stands for nonlinear complex conjugate control, which is the main contribution of this work and is conceived as a generalization of the ACC.

The main advantage of (45) as compared with (44) comes from the independence of the latter from the value of F. In general, F has an uncertain value even in cases where the monochromatic incident sea wave supposition can be considered sufficiently feasible.

Furthermore, by analyzing the ratio between the magnitudes of $b_r(\omega)$ and β the following two extreme scenarios can be identified.

- *Scenario 1: Negligible viscous damping* ($\beta << b_r(\omega)$)
  In this scenario the condition (43) leads to the damping adjustment for WECs with floaters with linear dynamics reported in [2, 23, 27]. This implies that the converted energy is maximized in the presence of monochromatic sea waves at frequency ω_p.
- *Scenario 2: Negligible radiation resistance* ($b_r(\omega) << \beta$)
  In this scenario the converted energy is maximized if the floater velocity satisfies

$$v(t) = v^*(t) = \text{sign}[F_w(t)]\left|\frac{F_w(t)}{3\beta}\right|^{\frac{1}{2}}. \tag{46}$$

The main difficulty for achieving such a floater velocity in the presence of irregular sea waves comes from the condition (41), which implies a strong dependence on the assumption of a narrow band around ω_p over $S(\omega)$. The condition (46), however, provides a simple criterion for adjusting β_g, as well as a possible reference signal for a tracking control strategy as an alternative to the impedance matching presented here.

4 | NUMERICAL VALIDATION AND DISCUSSION

To validate the proposed NCC scheme with the power maximization conditions (41) and (45), numerical simulations of the nonlinear WEC described by (16) were implemented in MATLAB/Simulink [28]. The synthetic experiments aimed to assess the performance of the system with the proposed impedance matching in the presence of deviations of the values of the damping coefficient β and the peak frequency of the incident wave ω_p. Regular sea waves as well as irregular sea waves were considered with the nominal values of the parameters in Table 1, in addition to the radiation resistance and the added mass shown in Figure 5. The irregular sea waves profiles were constructed according to the JONSWAP power spectrum shown in Figure 2.

TABLE 1 Parameter values [7, 18, 29].

Parameter	Value	Units
β_0	1.42×10^6	Ns^2/m^2
d_f	11	m
F	263.27	kN
H_1	2	m
g	9.81	m/s^2
m_f	0.4×10^6	kg
m_∞	0.2×10^6	kg
ω_{p0}	0.628	rad/s
ρ	1025	kg/m^3
S_f	70.88	m^2

The results are presented as follows. First, the time evolution of the floater velocity, the control law, and the converted power in nominal condition (i.e. $\beta = \beta_0$ and $\omega_p = \omega_{p0}$) are shown by using the NCC as well as the ACC adjustment of the damping to compare their performances. Second, by using the NCC, a performance measure derived from the average converted power is evaluated for deviations up to 25% of β and ω_p around β_0 and ω_{p0}, respectively.

By considering the condition (41), the shaping of the stiffness coefficient is done by assigning

$$\begin{aligned} k_g &= 0, \\ k &= k_s = \omega_{p0}^2[m_f + m_r(\omega_{p0})]. \end{aligned} \tag{47}$$

Regarding the shaping of the damping from Equation (43), the adjustment according to the proposed NCC is given by

$$\begin{aligned} \beta_g^{NCC} &= 2\beta_0, \\ b_g^{NCC} &= b_r(\omega_{p0}). \end{aligned} \tag{48}$$

On the other hand, to compare the proposed NCC with the traditional ACC, the following adjustment is used for the latter (also derived from Equation (43)):

$$\begin{aligned} \beta_g^{ACC} &= 0, \\ b_g^{ACC} &= \frac{2\sqrt{\pi b_r^2(\omega_{p0}) + 8F\beta_0} + \sqrt{\pi} b_r(\omega_{p0})}{3\sqrt{\pi}}. \end{aligned} \tag{49}$$

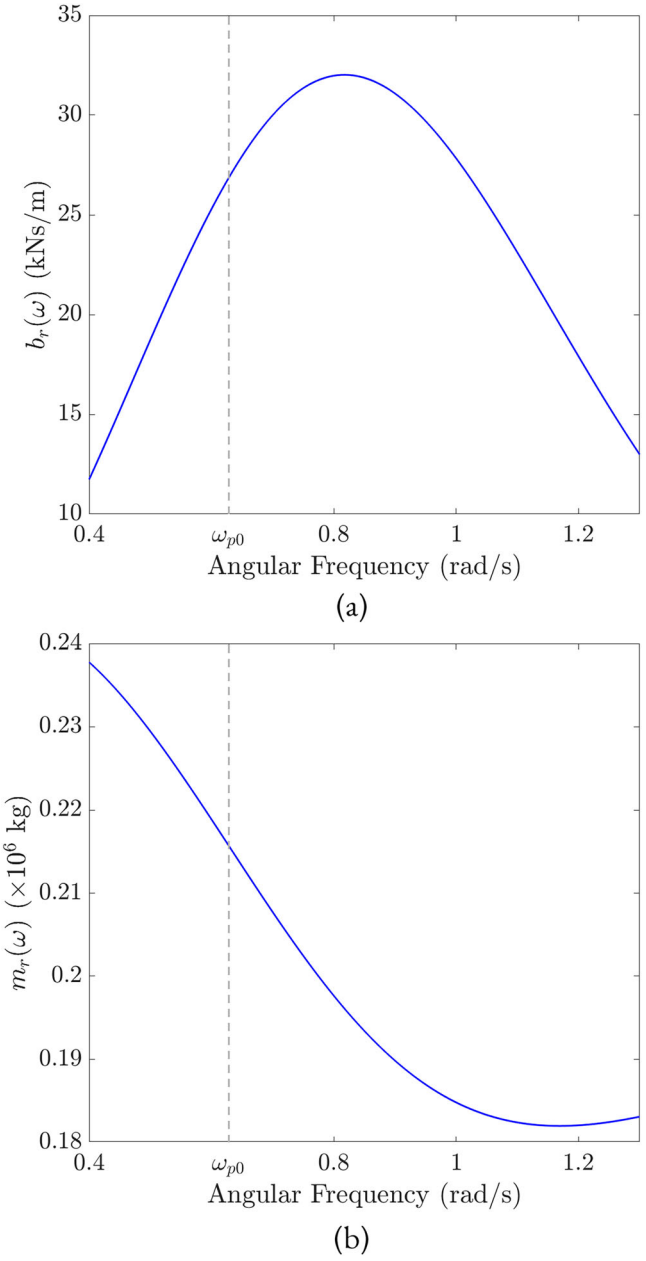

FIGURE 5 Frequency domain representation of (a) the radiation resistance and (b) the added mass of the WEC under study.

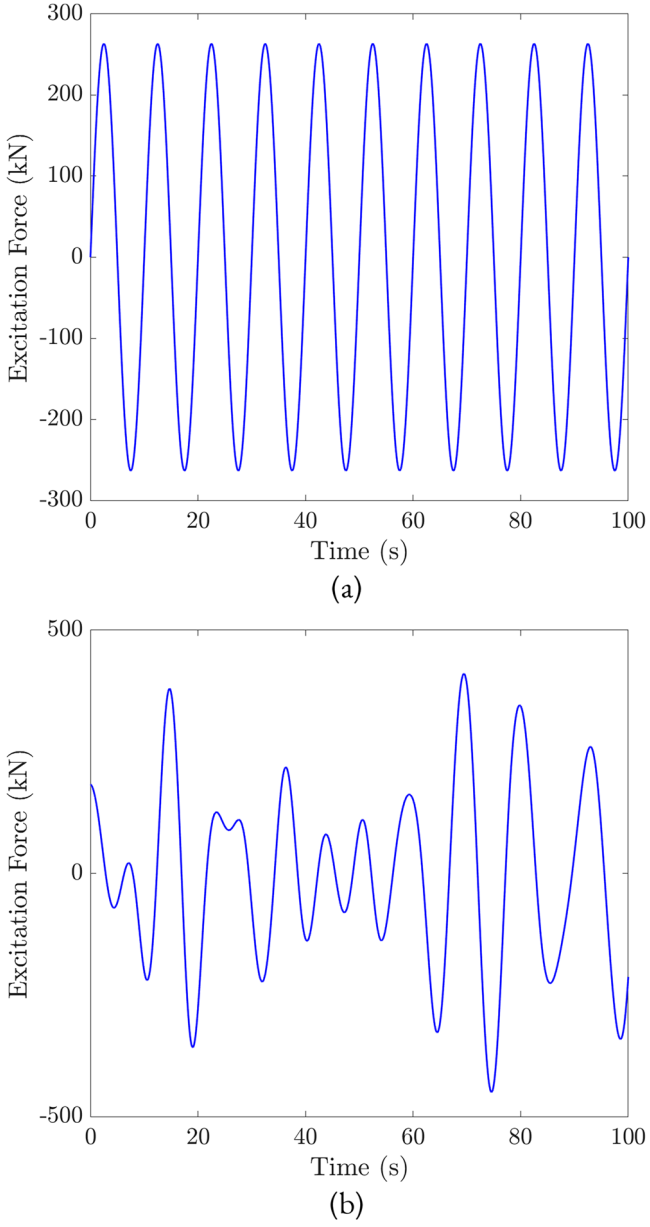

FIGURE 6 Simulated excitation force with (a) a regular sea wave and (b) an irregular sea wave.

4.1 | Comparison of the proposed NCC with linear ACC

The experiments shown in this subsection aim to compare the energy conversion by the WEC using the proposed NCC with that obtained with the usual ACC. To this end, one considers the profiles for the excitation force with $\omega_p = \omega_{p0}$ shown in Figure 6. For the regular sea wave case shown in Figure 6a, $F = 263.27$ kN was assigned. For the irregular sea wave, $H_1 = 2$ m was used as significant wave height for the JONSWAP power spectrum. The obtained excitation force time evolution for that case is shown in Figure 6b. It is worth noting that the value of F has been assigned to impose the same root mean square (RMS) value of $F_w(t)$ in the presence of regular and irregular sea waves, given $H1$ and ω_{p0}, during the time interval of 100 s shown in the graphs.

The first experiment simulated the behaviour of the WEC with the nominal values assigned for NCC and ACC. The time evolution of the floater velocity $v(t)$ with the systems with NCC and ACC are shown in Figure 7. The results in the regular and irregular sea wave scenarios are shown in Figures 7a and 7b, respectively. In addition, the time evolution of the instantaneous converted power,

$$p(t) = -u(t)v(t), \tag{50}$$

with both impedance matching methods is shown in Figure 8. The results with a regular sea wave and an irregular sea wave

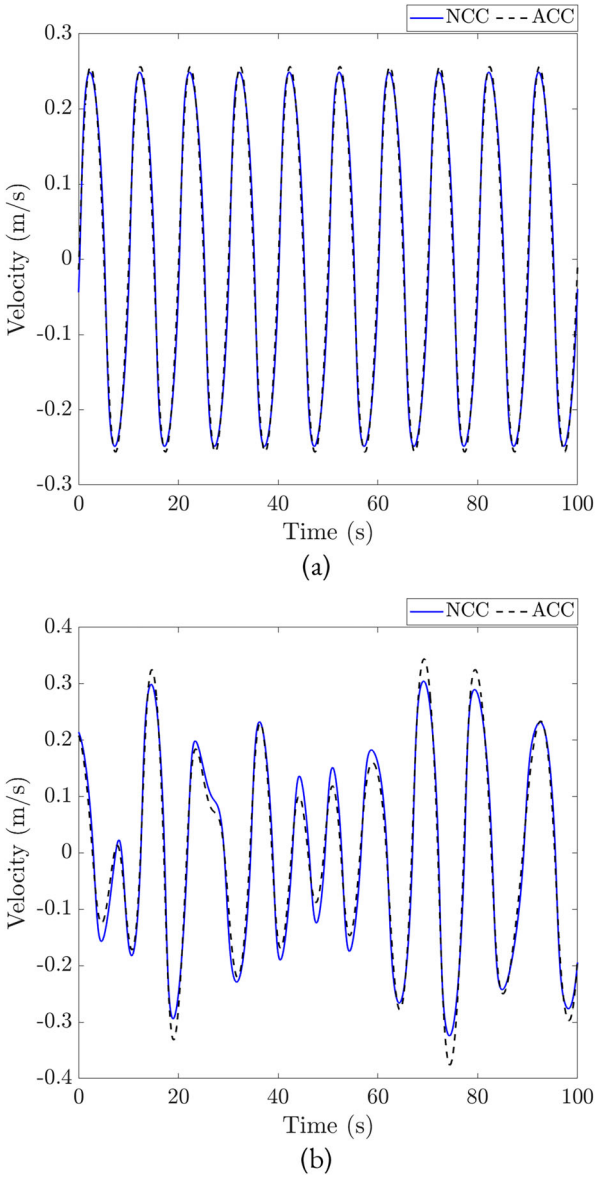

FIGURE 7 Time evolution of the floater velocity with (a) a regular sea wave and (b) an irregular sea wave.

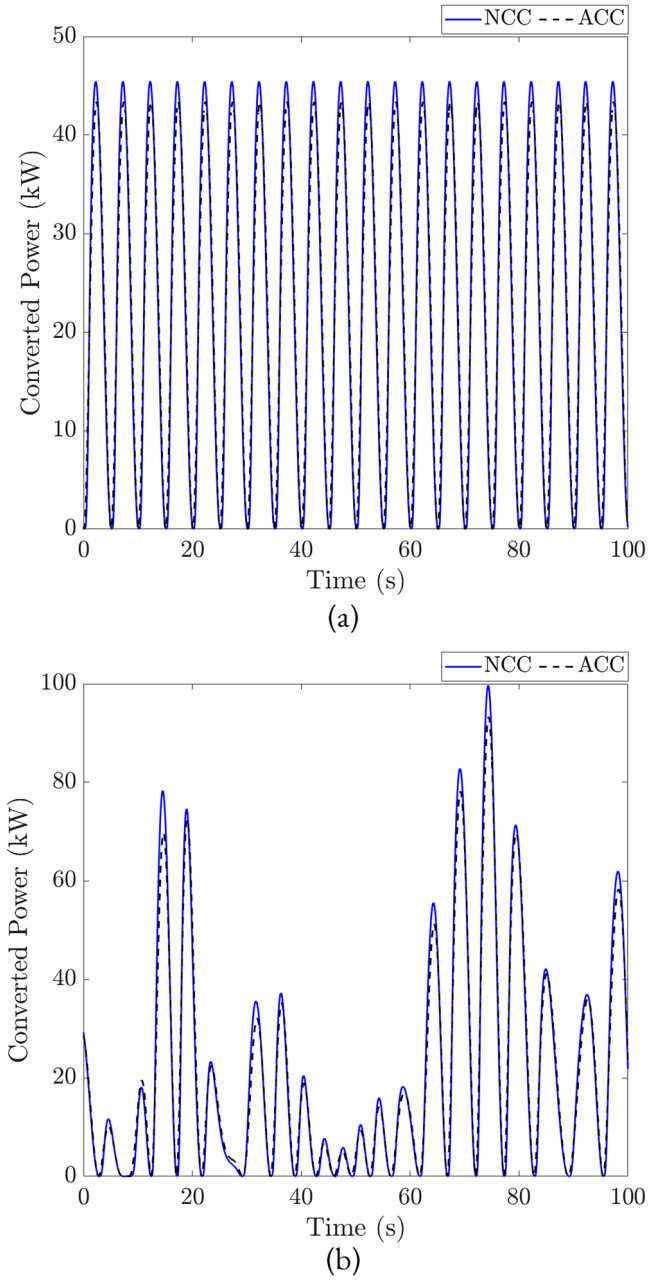

FIGURE 8 Time evolution of the instantaneous converted power with (a) a regular sea wave and (b) an irregular sea wave.

TABLE 2 Average converted power with NCC and ACC.

	Regular sea wave	**Irregular sea wave**
Average converted power with NCC (kW)	22.997	24.637
Average converted power with ACC (kW)	22.901	24.303

are shown in Figures 8a, 8b respectively. The obtained average converted power in each case is shown in Table 2.

The results of this experiment show that the system with proposed NCC provides greater average converted power in the presence of regular and irregular sea waves, even though the system with ACC demonstrates greater velocity extreme values. Even though the difference in the average converted power with both methods is below 5%, the amount of converted energy becomes more relevant for longer time intervals such as the ones desired for the continuous operation of the converter. This result shows an important feature in addition to the independence of the value of F for the NCC tuning.

The second experiment used several simulations for comparing both impedance matching methods by measuring the average converted power with different values of β_g^{NCC} and b_g^{ACC} around their nominal tuning used in the first experiment. Such a procedure seeks to validate the adjustment of both impedance matching methods by using (43), as well as by

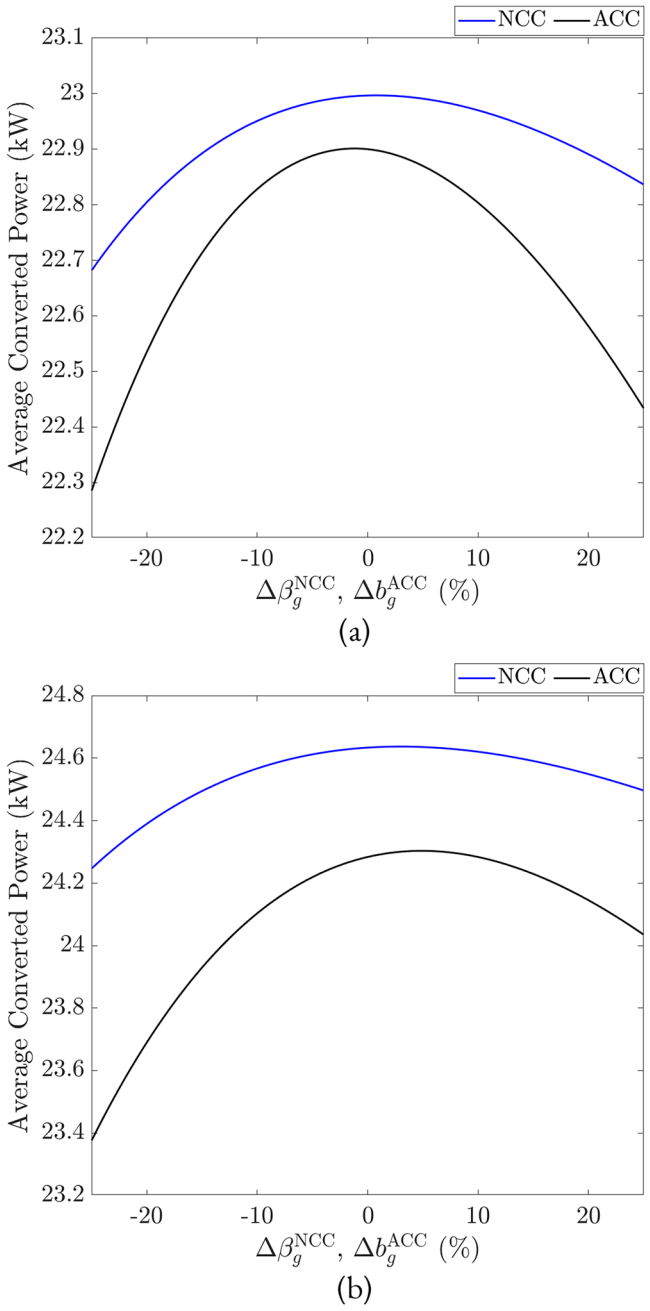

FIGURE 9 Average converted power with deviations of the main adjustments of NCC and ACC with (a) a regular sea wave and (b) an irregular sea wave.

checking if the system with NCC continues providing a greater energy conversion than the system with ACC given a different adjustment of both controllers. The results with regular and irregular sea waves are shown in Figure 9, where $\Delta\beta_g^{NCC}$ and Δb_g^{ACC} represent the variations of each parameter from their values assigned in (48) and (49), respectively.

The results of this experiment show that the adjustment of both impedance matching methods by using Equation (43) is close to their optimal values. This fact validates the use of the describing function method for deriving the mentioned impedance matching condition. In addition, the results confirm that the system with NCC provides a greater energy conversion even if the ACC is readjusted.

Since both experiments demonstrated a better performance of the system with NCC, the following experiments described in the next subsection aimed to study the robustness in the presence of deviations of the damping coefficient β as well as the peak period of the sea wave ω_p.

4.2 | Performance with deviations of the damping coefficient and the incident wave peak frequency

The experiments described in this section sought to evaluate the steady-state performance of the system with the proposed NCC impedance adjustment with the values given by (47) and (48) in the presence of uncertainty of the values of β and ω_p. This is accomplished by defining a performance index denoted as the average power ratio (APR), which is given by

$$\mathrm{APR}(\Delta\omega_p, \Delta\beta) = \left.\frac{P(b_g^{NCC}, \beta_g^{NCC}, k)}{P(b_g^*, \beta_g^*, k^*)}\right|_{\substack{\omega_p = \omega_{p0} + \Delta\omega_p \\ \beta = \beta_0 + \Delta\beta}}, \tag{51}$$

where $P(b_g^{NCC}, \beta_g^{NCC}, k)$ denotes the average converted power by using the nominal control and $P(b_g^*, \beta_g^*, k^*)$ is the average converted power for values of b_g, β_g, and k adjusted according to the actual values of ω_p and β:

$$\begin{aligned} b_g^* &= b_r(\omega_{p0} + \Delta\omega_p), \\ \beta_g^* &= 2(\beta_0 + \Delta\beta), \\ k_g^* &= 0, \\ k^* &= k_s^* = (\omega_{p0} + \Delta\omega_p)^2[m_f + m_r(\omega_{p0} + \Delta\omega_p)]. \end{aligned} \tag{52}$$

Note that according to the definitions above, one should obtain

$$\begin{aligned} &\mathrm{APR}(\omega_p, \beta) = 1 \quad \text{for} \quad \Delta\omega_p = \Delta\beta = 0, \text{ and} \\ &\mathrm{APR}(\omega_p, \beta) < 1 \quad \text{otherwise.} \end{aligned} \tag{53}$$

Thus, several simulations were performed with different values of β and ω_p by sweeping the region around β_0 and ω_{p0} given by

$$\begin{aligned} -0.25\beta_0 \le \Delta\beta \le 0.25\beta_0, \\ -0.25\omega_{p0} \le \Delta\omega_p \le 0.25\omega_{p0}. \end{aligned} \tag{54}$$

As mentioned above, for irregular sea waves a deviation of ω_p affects the shape of the power spectrum $S(\omega)$. The variations of $S(\omega)$ for the extreme cases considered here, $\omega_p = 0.75\omega_{p0}$ and $\omega_p = 1.25\omega_{p0}$, are shown in Figure 2.

The values of $\mathrm{APR}(\omega_p, \beta)$ obtained from the simulations are displayed in the surface graphs shown in Figure 10 as follows:

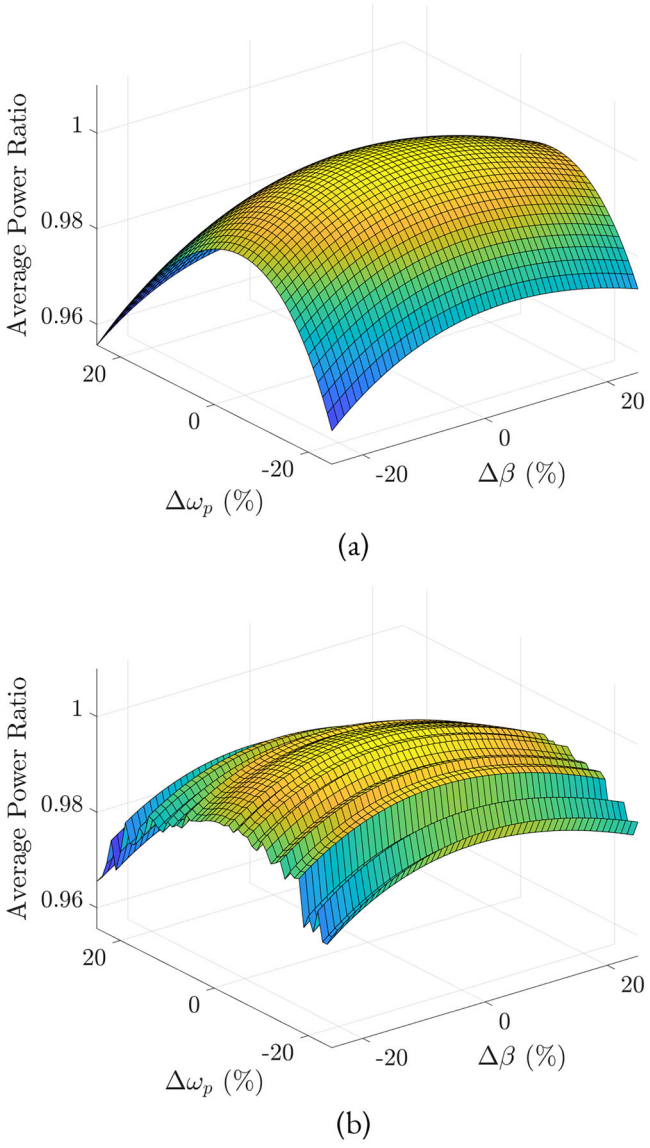

FIGURE 10 Average power ratio of the proposed impedance adjustment in the presence of deviations of ω_p and β with (a) a regular sea wave and (b) an irregular sea wave, with different random phase shifts for each value of ω_p.

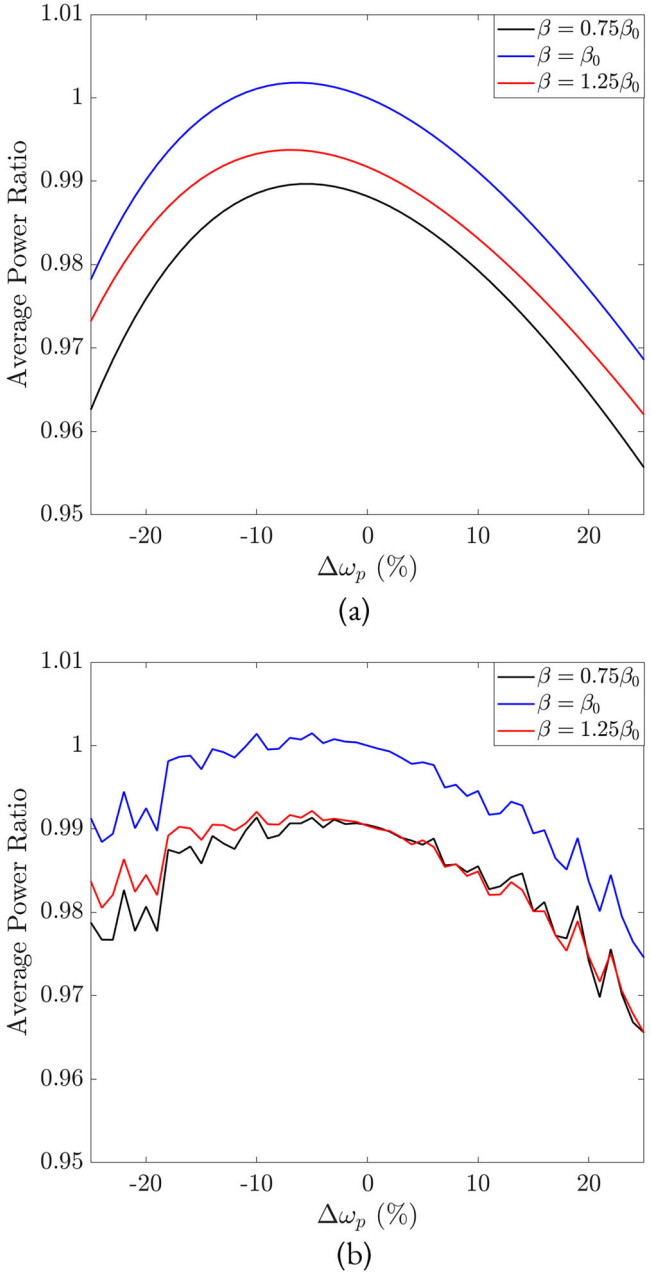

FIGURE 11 Average power ratio of the proposed impedance adjustment in the presence of deviations of ω_p with (a) a regular sea wave and (b) an irregular sea wave, for particular values of β.

Figure 10a shows the results with regular sea waves. Furthermore, Figure 10b shows results with irregular sea waves by assigning a random set of phase shifts φ_i for each wave profile obtained with each value of ω_p.

From the results in Figure 10, one can note that as expected $\text{APR}(\omega_p, \beta) \approx 1$ in the region around $\Delta\omega_p = 0$ and $\Delta\beta = 0$. The decrease of $\text{APR}(\omega_p, \beta)$ for extreme values of $\Delta\omega_p$ and $\Delta\beta$ resulted below 5% for the two simulated scenarios. The smooth surface obtained for the regular sea wave scenario comes from the absence of random phase shifts of adjacent harmonics for each value of ω_p, which are present with irregular sea waves.

To complement the analysis of the results in Figure 10, the effect of variations of ω_p on $\text{APR}(\omega_p, \beta)$ because of the nominal and deviated values of β (i.e. $\beta = \beta_0$, $\beta = 0.75\beta_0$, and $\beta = 1.25\beta_0$) is highlighted in Figure 11. The regular and irregular sea wave scenarios are shown in Figures 11a and 11b, respectively. As can also be seen in 10, the greater values of $\text{APR}(\omega_p, \beta)$ are obtained for $\beta = \beta_0$. For the regular sea wave scenario, $\text{APR}(\omega_p, \beta)$ is maximized for $\Delta\omega_p = -0.06\omega_{p0}$ instead of $\Delta\omega_p = 0$ as expected. This deviation can be attributed to the harmonic distortion caused by the nonlinear damping, which was neglected for the adjustment of k. Furthermore, it can be seen that the decrease in the $\text{APR}(\omega_p, \beta)$ for larger values of $\Delta\omega_p$ is larger for the regular sea wave scenario. This result can be related to the greater harmonic content of the irregular sea wave along with the band-pass filtering properties of the floater dynamics. Regarding this analysis, in Figure 2 one notes that for $\omega_p = 0.75\omega_{p0}$ the power spectrum $S(\omega)$ takes

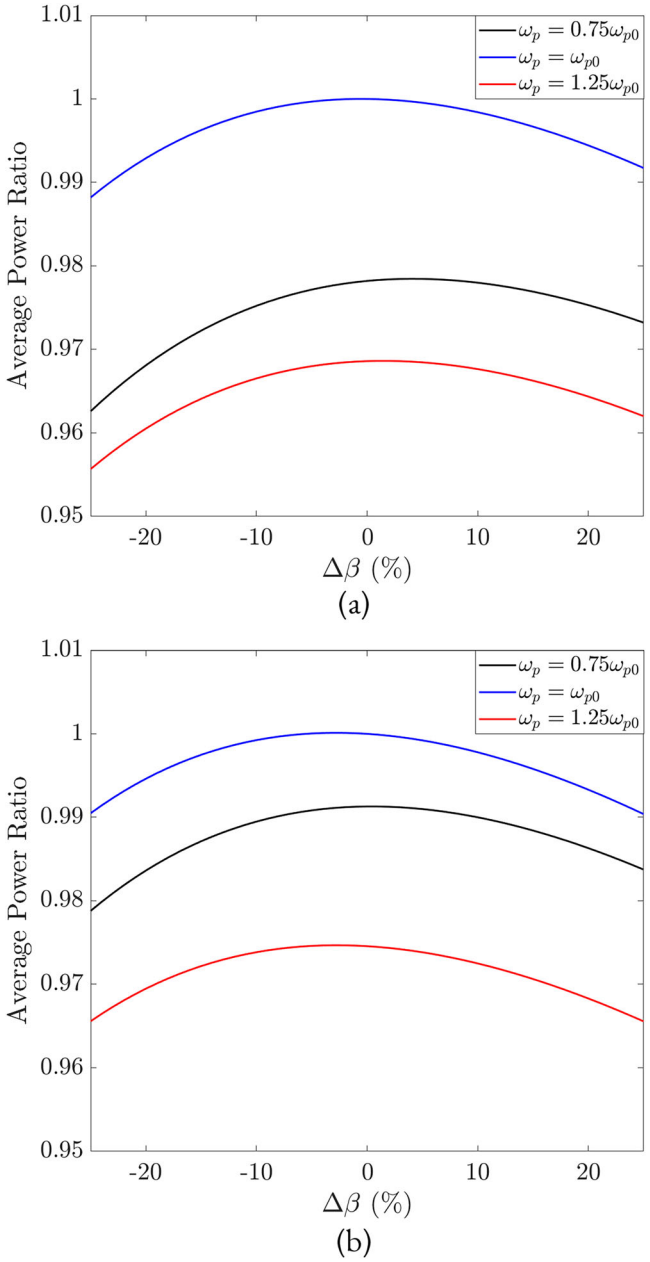

FIGURE 12 Average power ratio of the proposed impedance adjustment in the presence of deviations of β with (a) regular sea wave and (b) irregular sea wave, for particular values of ω_p.

greater values with respect to that with $\omega_p = 1.25\omega_{p0}$. This is also consistent with the asymmetrical variations APR(ω_p, β) noticeable in Figure 11b.

In addition, Figure 12 highlights the effect of variations of β on APR(ω_p, β) given the nominal adjustment and the values of ω_p (i.e. $\omega_p = \omega_{p0}$, $\omega_p = 0.75\omega_{p0}$, and $\omega_p = 1.25\omega_{p0}$). The regular and irregular sea wave scenarios appear in Figures 12a and 12b, respectively. In both scenarios one notes that the greater values of APR(ω_p, β) are obtained for $\omega_p = \omega_{p0}$. In the regular sea wave scenario, the value of $\omega_p = \omega_{p0}$ is maximized for $\beta = \beta_0$, while a minor deviation from this value can be seen in the presence of irregular sea waves. One can also ascertain the asymmetrical effect caused by deviations of ω_p mentioned above, which is greater in the irregular sea wave scenario.

5 | CONCLUSIONS

This study showed that a simple approximate NCC scheme derived from the describing function method allows improving the energy captured from regular and irregular sea waves. Such a method is a generalization of ACC that considers the effect of nonlinear damping. The simulation results showed that the proposed NCC yielded a greater amount of converted energy in comparison with that obtained with the ACC.

Even though the design procedure of the NCC only considered the presence of regular sea waves of known frequency, the results showed a robust performance within deviations of the peak frequency value of an irregular sea wave profile. This result verifies the assumption of a dominant frequency for applying the describing function method. A robust performance was also obtained within variations of the nonlinear damping coefficient.

The main advantage of the proposed NCC with respect to ACC is that its tuning does not depend on the amplitude of the incident sea wave. Information about the peak frequency of the wave and the nonlinear damping coefficient, however, remains an important requirement for obtaining an adequate mechanical impedance matching.

Further research will examine applying the proposed design method when a nonlinear stiffness force on the floater is considered, as well as estimating the nonlinear damping coefficient related to the drag force, which is not negligible in other wave energy converters.

AUTHOR CONTRIBUTIONS

Alejandro Gonzalez-Esculpi: Conceptualization, formal analysis, investigation, methodology, software, validation, writing - original draft, writing - review and editing. Cristina Verde: Conceptualization, formal analysis, funding acquisition, project administration, resources, supervision, writing - original draft, writing - review and editing. Paul Maya-Ortiz: Investigation, supervision, writing - review and editing.

CONFLICT OF INTEREST STATEMENT

The authors declare no conflicts of interest.

DATA AVAILABILITY STATEMENT

The data that support the findings of this study are available from the corresponding author upon reasonable request.

ORCID

Alejandro Gonzalez-Esculpi https://orcid.org/0000-0003-2346-2083

REFERENCES

1. Evans, D.V.: A theory for wave-power absorption by oscillating bodies. J. Fluid Mech. 77, 1–25 (1976)
2. Falnes, J.: Ocean Waves and Oscillating Systems: Linear Interaction including Wave-Energy Extraction. Cambridge University Press, Cambridge (2002)

3. Hals, J., Falnes, J., Moan, T.: A comparison of selected strategies for adaptive control of wave energy converters. J. Offshore Mech. Arctic Eng. 133(3), 031101 (2011)
4. Valério, D., Mendes, M.J., Beirão, P., Sá da Costa, J.: Identification and control of the AWS using neural network models. Appl. Ocean Res. 30(3), 178–188 (2008)
5. Davidson, J., Genest, R., Ringwood, J.V.: Adaptive control of a wave energy converter. IEEE Trans. Sustainable Energy 9(4), 1588–1595 (2018)
6. Jama, M., Wahyudie, A., Noura, H.: Robust predictive control for heaving wave energy converters. Control Eng. Pract. 77, 138–149 (2018)
7. Wu, F., Zhang, X., Ju, P., Sterling, M.J.H.: Modeling and control of AWS-based wave energy conversion system integrated into power grid. IEEE Trans. Power Syst. 23(3), 1196–1204 (2008)
8. Hansen, R.H.: Design and Control of the PowerTake-Off System for a Wave Energy Converter with Multiple Absorbers. Ph.D. thesis, Aalborg University (2013)
9. Song, J., Abdelkhalik, O., Robinett, R., Bacelli, G., Wilson, D., Korde, U.: Multi-resonant feedback control of heave wave energy converters. Ocean Eng. 127, 269–278 (2016)
10. Yu, Z., Falnes, J.: State-space modelling of a vertical cylinder in heave. Appl. Ocean Res. 17(5), 265–275 (1995)
11. Peña-Sanchez, Y., Windt, C., Davidson, J., Ringwood, J.V.: A critical comparison of excitation force estimators for wave-energy devices. IEEE Trans. Control Syst. Tech. 28(6), 2263–2275 (2020)
12. Genest, R., Ringwood, J.V.: A critical comparison of model-predictive and pseudospectral control for wave energy devices. J. Ocean Eng. Mar. Energy 2(4), 485–499 (2016)
13. Zhan, S., He, W., Li, G.: Robust feedback model predictive control of sea wave energy converters. IFAC-PapersOnLine 50(1), 141–146 (2017)
14. Nielsen, S.R., Zhou, Q., Kramer, M.M., Basu, B., Zhang, Z.: Optimal control of nonlinear wave energy point converters. Ocean Eng. 72, 176–187 (2013)
15. Giorgi, G., Ringwood, J.V.: Nonlinear Froude-Krylov and viscous drag representations for wave energy converters in the computation/fidelity continuum. Ocean Eng. 141, 164–175 (2017)
16. Ringwood, J.V.: Wave energy control: status and perspectives 2020. IFAC-PapersOnLine 53(2), 12271–12282 (2020)
17. Mérigaud, A., Ringwood, J.V.: Optimal trajectories, nonlinear models and constraints in wave energy device control. IFAC-PapersOnLine 50(1), 15645–15650 (2017)
18. Prado, M., Gardner, F., Damen, M., Polinder, H.: Modelling and test results of the Archimedes Wave Swing. Proc. Inst. Mech. Eng. Part A: J. Power Energy 220, 855–868 (2006)
19. Gelb, A., Vander Velde, W.E.: Multiple-Input Describing Functions and Nonlinear System Design. McGraw Hill, New York (1968)
20. Khalil, H.K.: Nonlinear Systems. Prentice Hall, Hoboken, NJ (2002)
21. Faltinsen, O.: Sea Loads on Ships and Offshore Structures, vol. 1. Cambridge University Press, Cambridge (1993)
22. Sergiienko, N., Cazzolato, B., Ding, B., Hardy, P., Arjomandi, M.: Performance comparison of the floating and fully submerged quasi-point absorber wave energy converters. Renewable Energy 108, 425–437 (2017)
23. Ringwood, J.V., Mérigaud, A., Faedo, N., Fusco, F.: An analytical and numerical sensitivity and robustness analysis of wave energy control systems. IEEE Trans. Control Syst. Tech. 28(4), 1337–1348 (2020)
24. Lee, C.-H.: WAMIT Theory Manual. Massachusetts Institute of Technology, Cambridge, MA (1995)
25. Babarit, A., Delhommeau, G.: Theoretical and numerical aspects of the open source BEM solver NEMOH. Paper published at the 11th European Wave and Tidal Energy Conference (EWTEC2015), Nantes, 5–11 September 2015
26. Frank, P.: Introduction to System Sensitivity Theory. Academic Press, New York (1978)
27. Ringwood, J.V., Bacelli, G., Fusco, F.: Energy-maximizing control of wave-energy converters: the development of control system technology to optimize their operation. IEEE Control Syst. Mag. 34(5), 30–55 (2014)
28. MATLAB.: version 9.5 (R2018b). The MathWorks Inc., Natick, Massachusetts (2018). https://www.mathworks.com
29. Gieske, P.: Model predictive control of a wave energy converter: Archimedes wave swing. Master's thesis, Delft University of Technology (2007)

How to cite this article: Gonzalez-Esculpi, A., Verde, C., Maya-Ortiz, P.: Nonlinear impedance matching control for a submerged wave energy converter. IET Control Theory Appl. , 1–14 (2023). https://doi.org/10.1049/cth2.12565